Characterization of Fading on Fixed Wireless Channels between 200 MHz and 2 GHz in Suburban Macrocell Environments

Anthony Liou, *Student Member, IEEE,* Kyle N. Sivertsen, *Student Member, IEEE,* Pouyan Arjmandi, Ganapathy Viswanathan, Boubacar Diallo, Sol Lancashire, and David G. Michelson, *Senior Member, IEEE*

***Abstract*—Growing use of point-to-multipoint fixed wireless networks to support network access and SCADA applications in suburban macrocell environments has prompted regulators to re-allocate various bands between 200 MHz and 2 GHz to such applications. Links in such networks are usually obstructed by buildings and foliage and are classified as non-line-of-sight. Although it is well-known that such links are susceptible to fading caused by windblown trees and foliage, most past efforts to characterize fading on such links have focused on frequency bands at 1.9 GHz and above. Here, we show how signal fading in the 220, 850 and 1900 MHz bands vary with both distance and time-averaged wind speed in a representative macrocell environment. Based upon time-series of received signal strength collected in a typical macrocell environment with moderate foliage at locations between 1 and 4 km from a transmitting site located 80 m above ground level, we show that fading on such links is relatively severe at 1.9 GHz but decreases rapidly as the carrier frequency decreases. We have expressed our results in the form of a first-order simulation model. Additional data will be required to estimate standardized model parameters that can be applied to a broad range of environments.**

***Index Terms*—Channel model, fading channels, macrocell environment, radiowave propagation, radiowave propagation - meteorological factors.**

I. Introduction

DEPLOYMENT of fixed wireless communications systems in suburban environments has attracted considerable interest in recent years as: (1) common carriers seek methods for providing either fixed or nomadic network access services to residential households without the expense of deploying wireline connectivity over the last mile [1], [2] and (2) as public utilities begin to deploy smart meters and related devices in residential neighbourhoods in order to: (a) detect and report outages, (b) monitor usage, (c) implement strategies that encourage customers to limit and/or time-shift their demand for power and (d) implement finer control over the distribution grid [3]-[5]. In macrocell environments, *i.e.*, environments in which the base station antenna is mounted well above the local rooftop or treetop level and the remote terminal antenna is mounted below the local rooftop or treetop level, wireless links are usually obstructed by intervening obstacles and most of the signal that reaches the receiver does so as a result of scattering and diffraction by objects in the environment. Because both the transmitting and receiving antennas in such applications are fixed, signal fading is caused solely by the motion of objects in the environment that scatter and diffract the signal. In suburban macrocell environments, a large fraction of those objects are trees and foliage with leaves and branches that sway when blown by the wind.

During the past decade, groups in Canada, the United States, the United Kingdom, Chile, Australia and elsewhere have conducted measurement campaigns aimed at characterizing the manner in which signal fading occurs on non-line-of-sight (NLOS) paths in macrocell environments, e.g., [6]-[13]. Such studies have variously sought to characterize: (1) the first-order statistics of the fading signal envelope over time and location, (2) the rate at which the signal fades, either through direct estimation of the Doppler spectrum or through estimation of the average fade duration and level crossing rate, (3) the effect of the height and beamwidth of the receiving antenna, local density of vegetation and the wind speed in the vicinity, and (4) the performance of space and polarization diversity at either the base station or the remote terminal.

The vast majority of previous studies of fixed wireless channels in suburban macrocell environments focused on individual frequency bands at 1.9 GHz and above, including the PCS band at 1.9 GHz, the ISM band at 2.45 GHz, the Fixed Wireless Access (FWA) band at 3.5 GHz and the U-NII and ISM bands at 5.2 and 5.8 GHz. However, spectrum regulators have recently begun to reallocate frequency bands below 2 GHz in order to help meet the requirements for broadband wireless access for urban and rural areas and/or narrowband telemetry for public utilities. In Canada, spectrum in frequency bands near 220 MHz, 700 MHz and 1430 MHz have either been proposed for, or designated for, use in utility telemetry and automation of the electrical power grid [14] while spectrum in frequency bands near 700 MHz has also been proposed for fixed wireless broadband use in rural areas [15]. Regulators are increasingly designating multiple primary allocations within

Manuscript received July 6, 2009; revised August 5, 2009; accepted August 10, 2009. The associate editor coordinating the review of this paper and approving it for publication was C. Xiao.

A. E.-L. Liou, K. N. Sivertsen, and D. G. Michelson are with the Department of Electrical and Computer Engineering, University of British Columbia, Vancouver, BC, Canada, V6T 1Z4 (e-mail: {ksiverts, eliou, davem}@ece.ubc.ca).

P. Arjmandi is with GrowthWorks Capital Ltd., 2600 - 1055 West Georgia Street Vancouver, BC V6E 3R5.

G. Viswanathan is with Matrikon Inc., 10405 Jasper Avenue, Edmonton, AB, Canada T5J 3N4.

S. Lancashire and B. Diallo are with BC Hydro, 6911 Southpoint Drive Burnaby, BC V3N 4X8.

This work was supported in part by grants from Western Economic Diversification Canada, Bell Canada, BC Hydro, and Tantalus Systems.

Digital Object Identifier 10.1109/TWC.2009.091004

individual frequency bands, as well as proposing more flexible licensing schemes, in an attempt to accommodate different users and services in the same spectrum. RF spectrum below 2 GHz that has traditionally been used for broadcasting and fixed point-to-point applications is increasingly being transferred to mobility and fixed point-to-multipoint applications. Thus, the amount of radio spectrum, and the choice of frequency bands available for fixed point-to-multipoint applications, will almost certainly increase in coming years.

The manner in which path loss, or its reciprocal, path gain, is affected by the carrier frequency, the heights of and separation between the base station and mobile terminal in suburban macrocell environments over the range from 200 MHz to 2 GHz has been well-studied over the years and has been captured by several standard models [16]-[18]. However, existing channel models do not provide a description of the depth of signal fading that fixed wireless channels will experience over this frequency range in suburban macrocell environments. (Ref. [19] describes fading on UHF links between fixed nodes within a tropical rain forest but the link configuration (both nodes were located below the forest canopy) was quite different from that encountered in suburban macrocells.) This lack of information places those charged with planning, simulating or deploying fixed wireless systems in suburban macrocell environments at a severe disadvantage when asked to predict system coverage and outage probabilities.

Here, we take the first steps to develop a measurement-based fading channel model suitable for use across the frequency range from 200 MHz to 2 GHz. We established a transmitting site atop an eighteen-storey office tower located in the middle of a large suburban area. We simultaneously broadcast single carrier signals in the 220, 850 and 1900 MHz bands and collected time-series of the received signal strength observed in each band at fixed locations at ranges between 1 and 4 km. We reduced the data in order to determine the manner in which path gain and signal fading vary with distance, time-averaged wind speed and carrier frequency in a typical suburban macrocell environment. The resulting measurement-based model allows one to compare the coverage and outage probability that links at different frequencies would experience in a typical macrocell environment. The frequencies that we employed bracket the majority of the bands that either have been, or are likely to be, allocated to fixed wireless access, SCADA (supervisory control and data acquisition) and Smart Grid applications. Although our results strictly apply to narrowband channels, they are also relevant to single carriers in multicarrier modulation schemes. The results presented here are specific to high transmitting sites; in future work, we shall determine how lowering the base station height affects the results.

The remainder of this paper is organized as follows: In Section II, we summarize the essential aspects of our first-order model of fading on narrowband channels. In Section III, we describe our measurement setup and test site. In Section IV, we present our results. In Section V, we show how these results can be used in system-level simulations. In Section VI, we discuss the implications of the results and summarize our findings and contributions.

II. The Narrowband Fading Channel Model

The essential aspects of fading on narrowband fixed wireless channels have been described previously in [6], [7] and [20]. The complex signal path gain of a narrowband channel (typically tens of kHz wide) over a given time interval (typically several minutes long) is given by

$$g(t) = V + v(t) \tag{1}$$

where V is a complex number and $v(t)$ is a complex, zero-mean random time variation caused by wind-blown foliage, vehicular traffic, etc. Both V and the parameters of the random process $v(t)$ may change from one time segment to another.

From time series data collected over a given time-frequency segment, we can calculate the average power gain

$$G = \overline{|g(t)|^2} = |V|^2 + \overline{|v(t)|^2} = |V|^2 + \sigma^2 \tag{2}$$

where σ^2 is the variance of the complex Gaussian process $v(t)$. The rms fluctuation of the envelope about the mean is given by the standard deviation of $|g(t)|^2$ and is denoted by σ_G. Because $v(t)$ is a complex Gaussian process, the distribution of $|g(t)|^2$ over time is Ricean. The K-factor of the distribution is given by

$$K = |V|^2 / \overline{|v(t)|^2} = |V|^2/\sigma^2. \tag{3}$$

Various methods for estimating K have been proposed; we use the moment-based method described in [20] where

$$K = \frac{|V|^2}{\sigma^2} = \frac{\sqrt{G^2 - \sigma_G^2}}{G - \sqrt{G^2 - \sigma_G^2}}. \tag{4}$$

In terms of G and K, the expression for $g(t)$ in (1) can be re-cast as

$$g(t) = \sqrt{\frac{G}{K+1}} \left[\sqrt{K} e^{j\Psi} + x(t) \right], \tag{5}$$

where Ψ is the phase of V and $x(t)$ is a zero-mean complex Gaussian process with a unit standard deviation. From (5), the channel parameters G and K completely specify the first-order statistics of the signal at a given location over time intervals of several minutes.

Knowledge of the first order statistics of signal fading is sufficient to predict the probability of the link experiencing a given fade depth or outage. Further, it has been observed that the level of cross-polar discrimination (XPD) on the channel is highly correlated with the Ricean K-factor [21]. Previous measurements in suburban macrocell environments at frequencies above 1.5 GHz have shown that on Ricean channels, G and K are both well-modeled by Gaussian distributions when they are expressed in dB, *e.g.*, [6]. The implication of this result is that these parameters can be modeled and simulated as a set of Gaussian variates whose joint distribution is completely determined by their means, standard deviations and mutual correlation coefficients. In the sections that follow, we describe our efforts to characterize the parameters of this first-order model in a typical suburban macrocell.

III. The Measurement Setup

A. Tri-band Channel Sounder

Our tri-band channel sounder consists of a multiband continuous wave (CW) transmitter and receiver that operate in the 220, 850 and 1900 MHz frequency bands. The signal source portion of the transmitter contains a pair of Marconi 2022 RF signal generators, each of which is capable of supplying a CW signal up to 6 dBm over the range 10 kHz to 1 GHz, and a Marconi 2031 RF signal generator capable of supplying a CW signal up to 13 dBm over the range 10 kHz to 2.7 GHz. The signal generators are locked to a 10 MHz reference signal supplied by a Stanford Research Systems PRS10 Rubidium frequency standard. It, in turn, is disciplined by the 1 PPS signal supplied by a Trimble Resolution-T GPS receiver that has been designed for such applications.

The amplifier portion contains three power amplifiers: (1) a TPL Communications LMS series RF power amplifier capable of delivering up to 100 W at 220 MHz, (2) a Unity Wireless Dragon RF power amplifier capable of delivering up to 30 W between 869 and 894 MHz and (3) a Unity Wireless Grizzly RF power amplifier capable of delivering up to 35 W between 1930 and 1990 MHz. During data collection, all three amplifiers were configured to deliver 20 W signals to their respective feedlines. A wireless remote control device that operates near 150 MHz allowed the data collection team to remotely enable or disable the power amplifiers at the start or end of a measurement session. The 220, 850 and 1900 MHz transmitting antennas are vertically polarized, omnidirectional and have gains of 8.1, 6.1 and 5.0 dBi, respectively. They were installed atop the eighteen-storey office tower at BC Hydro's Edmonds facility in Burnaby, BC at a height of 80 m above ground level. The remaining parameters used in the system link budget for each band are given in Table I.

The receiving antennas are also vertically polarized and omnidirectional; the 850 MHz and 1900 MHz antennas are half-wave coaxial dipoles which present a gain of 2.2 dBi while the 220 MHz antenna is a quarter-wave monopole that presents a gain of 5.2 dBi. When used in NLOS configurations, fixed wireless antennas are typically mounted at heights between 0.5 m (e.g., for nomadic applications) and 4 m (*e.g.*, for permanent installations). As a compromise, we mounted the antennas on the roof of our propagation measurement van at a height of 2.3 m. In many cases, fixed wireless antennas are directional. Because our primary objective is to compare the behaviour of the channel at different frequencies, we elected to simplify the data collection protocol by collecting the measurement data using omnidirectional antennas. If the remote terminal antenna's beamwidth decreases or its height is increased, the path gain and/or the Ricean K-factor will tend to increase [7].

Our multiband receiver consists of: (1) a pair of Anritsu MS2651B spectrum analyzers that operate over the range of 9 kHz to 3 GHz with a selectable IF bandwidth, (2) an Anritsu MS2721A spectrum analyzer that operates over the range of 100 kHz to 7.1 GHz with a selectable IF bandwidth, (3) a Stanford Research Systems PRS10 Rubidium frequency standard that generates a 10 MHz reference signal to which the spectrum analyzers can be locked and (4) a Trimble Resolution-T GPS receiver that supplies the 1 PPS signal used to discipline the frequency standard. External low-noise preamplifiers with 30 dB and 26 dB gain were used to increase the sensitivity of the spectrum analyzers that measure the received strength of the 850 and 1900 MHz signals, respectively. We used a laptop computer equipped with a GPIB adapter to: (1) configure the spectrum analyzers and (2) collect data from them. We geocoded the data with a nominal circular error probability (CEP) of less than 5 metres using location information supplied by a u-blox Antaris 4 SuperSense GPS receiver.

TABLE I
Link Budget Parameters for the Tri-band Channel Sounder.

Parameter	220 MHz	850 MHz	1900 MHz
Transmitted Power	43 dBm	43 dBm	43 dBm
Transmit Cable Loss	1.3 dB	2.7 dB	4.3 dB
Transmit Antenna Gain	8.1 dBi	6.1 dBi	5 dBi
Receive Antenna Gain	5.2 dBi	2.2 dBi	2.2 dBi
Receive Cable Loss	0.37 dB	0.76 dB	1.2 dB
Receiver LNA Gain	-	30 dB	26 dB

B. Verification Protocol

Before we collected any field data, we verified the function and operation of our tri-band CW channel sounder using a Spirent SR5500 channel emulator. We set the relevant narrowband channel parameters, including path gain and Ricean K-factor, to various values over a broad range and, in each case, confirmed that we were able to correctly estimate each of the parameters. We verified the transmitted power levels using a Bird Model 5000EX digital wattmeter.

C. Weather Instruments

We measured the wind speed, wind direction, rain rate and outdoor temperature using a Davis Vantage Pro 2 wireless weather station that we mounted on a mast located about 30 metres away from the transmitting antennas. Internally, the weather station samples the relevant weather parameters every few seconds. Once per minute, it logs the average values of these parameters over the previous minute to an internal database. We used a custom software tool to match the received signal strength data collected at a given time and location to the relevant weather data. Because previous work has shown that variations in average wind speed at tree top level or above are well correlated over mesoscale distances of several kilometers [22], they provide a reasonable description of aggregate conditions along a given path. Thus, we concluded that collecting wind data at a single location near the base station would be adequate for our purposes.

D. Test Area

Our test area consisted of suburban neighbourhoods with generally flat terrain, light to moderate foliage and one- and two-storey houses. We collected measurement data at 84 fixed measurement locations that were situated within an annulus between 1 and 4 km from the transmitter site. Almost all the motion in the environment arose from windblown foliage; few,

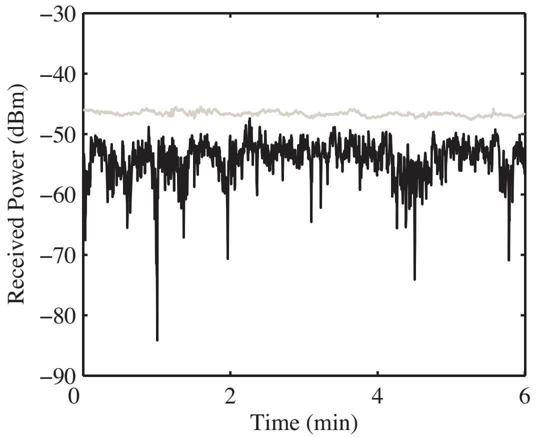

Fig. 1. Typical time series of received signal strength at 220 MHz (top) and 1900 MHz (bottom) with Ricean K-factors of 24.2 and 7.4 dB, respectively.

if any, cars, people or other moving scatterers were in the vicinity when we collected measurement data. Most of the foliage in the area is deciduous and between 4 and 7 m in height but at least one-third is coniferous and up to 15 m in height. The duration of the measurement campaign was too short to permit observation of the effects of seasonal variations in the foliage. All of our data was collected with leaves on the trees.

E. Data Collection Protocol

Our data collection protocol comprised the following steps. First, we conducted a rapid survey of the proposed measurement locations in order to ensure that the strength of the received signal would be at least 10 dB above the noise floor at all locations. Next, over a span of several days, the operator drove the propagation measurement van to each of the fixed measurement locations that we had selected in advance. At each location, the operator collected simultaneous time series of the received strength of the 220, 850 and 1900 MHz CW signals. The measured data were collected in the form of three successive 120 second sweeps. For the two upper bands, the pair of Anritsu MS2651B spectrum analyzers were used to record three sweeps of 501 samples each, yielding 1503 received signal strength samples at each location. For the 220 MHz band, the Anritsu MS2721A spectrum analyzer was used; it yielded 551 samples per sweep or 1653 samples at each location.

Time-series recordings of received signal strength of 6 minutes in duration as measured at a typical location at a distance of 1.44 km from the transmitting site are shown in Figure 1. The upper trace is the 220 MHz received signal; its average received signal strength is -47 dBm and its Ricean K-factor is 24.2 dB. The lower trace is the 1900 MHz received signal; its average received signal strength is -53 dBm and its Ricean K-factor is just 7.4 dB. These K-factor values are very similar to the averages over all locations at each of the two frequencies. The greater severity of the signal fading at 1900 MHz compared to 220 MHz is apparent.

IV. Results

A. Distribution of Ricean K-factors

Over the 84 measurement locations and in all three frequency bands, virtually all of the received signal time series experience fading distributions that are well approximated by Ricean distributions. We observed that 95% of the time series are stationary over the six-minute duration, *i.e.*, they display consistent depth and rate of fading over the entire sample. The marginal distributions of the Ricean K-factors in each band tend to follow a lognormal distribution (*i.e.*, normal in dB), as suggested by Figure 2. (When we claim or imply that a parameter or residual follows a Ricean distribution, we mean that it passed the Kolmogorov-Smirnov goodness-of-fit test at the 5% significance level. For normal or lognormal distributions, we apply the Anderson-Darling test instead.) The mean values of K decrease as the carrier frequency increases: $\overline{K}_{220} = 23 \pm 1.66$ dB $>>$ $\overline{K}_{850} = 11.2 \pm 1.55$ dB $> \overline{K}_{1900} = 7.7 \pm 1.57$ dB, where the estimated values are given with their 95% confidence intervals. The corresponding standard deviations are much more similar to each other with $\sigma_{220} = 8.3$ dB, σ_{850} =6.6 dB, σ_{1900} =6.8 dB. The results at 1900 MHz are consistent with those reported by others, including [7].

Although our results are only based upon three frequencies, we made a preliminary attempt to use linear regression analysis based on the least squares approach to determine the relationship between $\overline{K}$ and the carrier frequency. The resulting regression line is shown in Figure 3 and is given by

$$\overline{K}(\mathrm{dB}) = -16.6\log_{10}(f) + 61.5 \qquad (6)$$

where $\overline{K}$ is expressed in dB and the carrier frequency f is expressed in MHz. The variability of K over all locations at each frequency is remarkably similar and falls between 6.8 and 8.3 dB, a range of less than 1.5 dB. Although these results should be regarded as preliminary because they are based upon only three frequencies, the trend is consistent with the notion that $\overline{K}$ is inversely proportional to $\log_{10}(f)$. It also suggests that the frequency dependence of $\overline{K}$ should be investigated further.

If, as seems likely, the time-varying component of the received signal is the result of scattering by windblown trees and foliage, the frequency dependence of the severity of fading can likely be explained by considering the displacement of the moving scatterers in terms of the wavelength of the signal. As wavelength increases, a given displacement of leaves and branches by the wind will lead to a much smaller phase shift of the scattered signal and a much lower probability of deep fades occurring at the receiver. Efforts to formulate physical models capable of predicting and/or simulating fading on fixed wireless channels due to moving vegetation were reported in [23], [24] and [25]. However, all were based upon or validated using fading channel measurements collected at 2 GHz or above. An obvious next step is to develop more sophisticated physical models that capture the frequency dependence of fading due to moving vegetation at frequencies below 2 GHz.

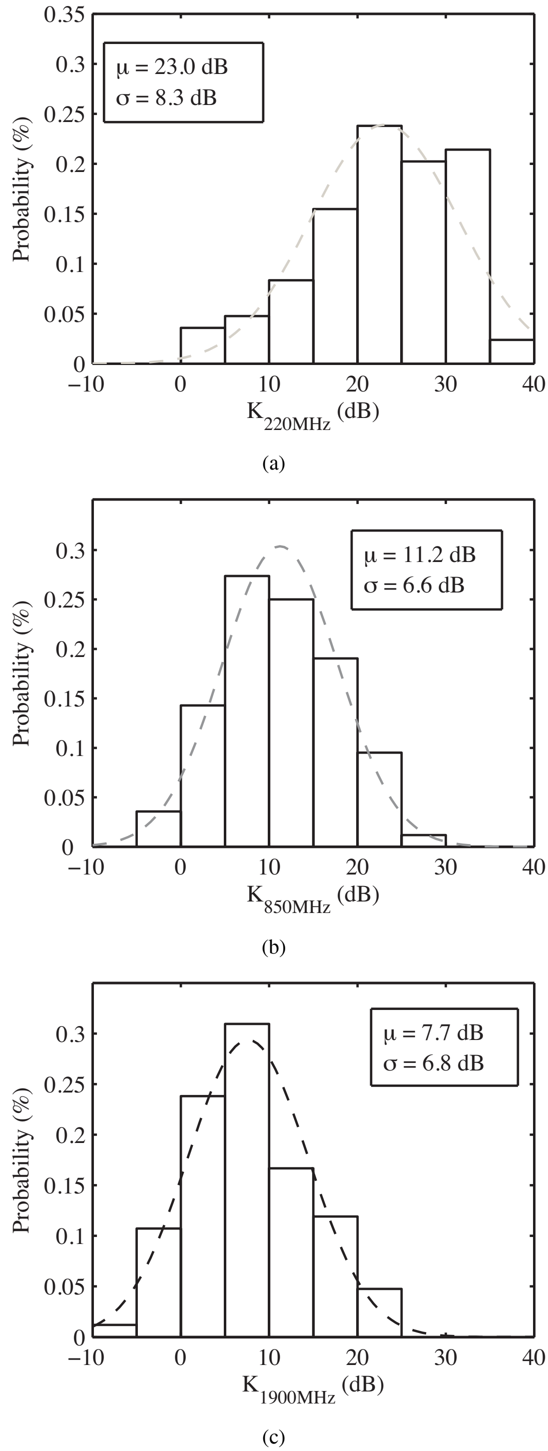

Fig. 2. Distribution of Ricean K-factors observed throughout the test area at (a) 200MHz, (b) 850MHz, and (c) 1900MHz.

B. Path Gain and Ricean K-factor vs. Distance

We used (2) and (4) to estimate the values of G and K, respectively, that describe the set of time series data collected at each location, then plotted the results vs. the distance between the transmitter and the receiver. Path gain and Ricean K-factor both decrease with distance according to a power law relationship as suggested by Figures 4(a) and (b). We characterized the distance dependence of G and K by estimating the regression line that best fits the measured data in a least squares sense. We also estimated the value of Pearson's correlation coefficient ρ between each parameter and distance d and estimated the location variability σ of the parameter, *i.e.*, the standard deviation of the residuals. The regression lines for G and K and the corresponding correlation coefficients ρ and location variabilities σ in each frequency band are given by

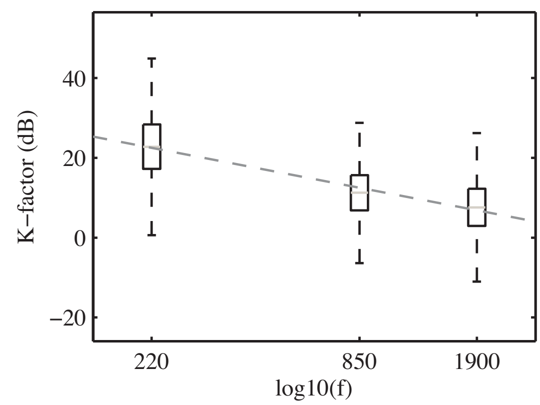

Fig. 3. Regression analysis of Ricean K-factors vs. carrier frequency in MHz. The distribution of K at 220, 850 and 1900 MHz is indicated by a box plot.

$$\overline{G}_{220}(\mathrm{dB}) = -33.5\log_{10}d - 90.5;\ \rho = -0.59, \sigma = 7.2, \quad (7)$$

$$\overline{G}_{850}(\mathrm{dB}) = -37\log_{10}d - 109.6;\ \rho = -0.64, \sigma = 6.9, \quad (8)$$

$$\overline{G}_{1900}(\mathrm{dB}) = -36\log_{10}d - 115.9;\ \rho = -0.58, \sigma = 7.9, \quad (9)$$

and

$$\overline{K}_{220}(\mathrm{dB}) = -8.0\log_{10}d + 25.8;\ \rho = -0.15, \sigma = 8.3, \quad (10)$$

$$\overline{K}_{850}(\mathrm{dB}) = -4.9\log_{10}d + 12.9;\ \rho = -0.12, \sigma = 6.5, \quad (11)$$

$$\overline{K}_{1900}(\mathrm{dB}) = -8.5\log_{10}d + 10.5;\ \rho = -0.19, \sigma = 6.7, \quad (12)$$

respectively, where each parameter's subscript indicate the relevant frequency band in MHz and all values of σ are given in dB. For simplicity, subscripts have not been added to either ρ or σ; it is understood that each instance applies only to the corresponding regression line. Pearson's correlation coefficient provides a useful indication of the goodness of fit of the line and our confidence in the estimates of the slope and intercept of the regression line. Path gain changes with distance and frequency in the general manner predicted by standard models. The distance coefficients in (7)-(9) are 33.5, 37 and 36, respectively. They are higher than but comparable to the value of 32 that the Okumura-Hata/COST-231 model predicts for a high transmitting site and light-to-moderate foliage with gentle terrain in the coverage area [16],[17]. They are also consistent with the AT&T suburban path loss model presented in [18]. We also note that the exponent increases slightly as the frequency increases. In general, approximately two-thirds of the differences in path gain (in dB) between frequencies can be attributed to the reduction in the effective area of the receiving antenna at higher frequencies. The remaining third can likely be attributed to increased diffraction losses as the frequency increases. For a given distance d, $\overline{K}_{220}(d) >> \overline{K}_{850}(d) > \overline{K}_{1900}(d)$, which is consistent with

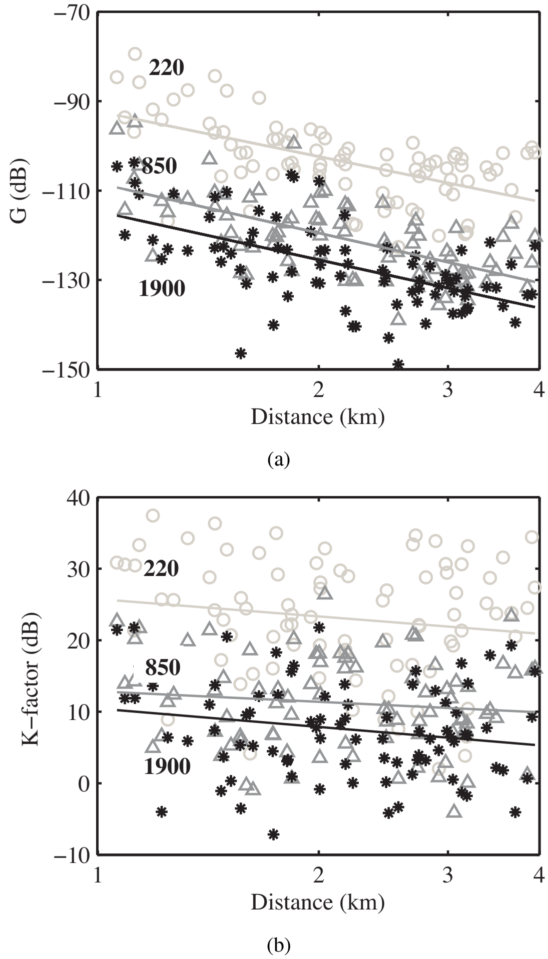

Fig. 4. (a) Average path gain G and (b) Ricean K-factors observed at 220 (○), 850 (△), and 1900 (●) MHz vs. distance.

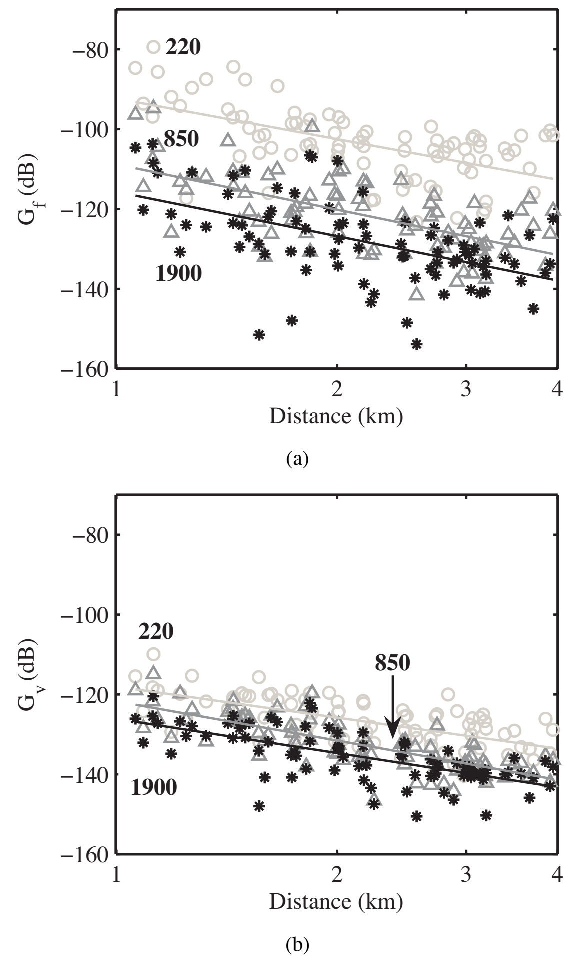

Fig. 5. (a) Fixed path gain G_f and (b) time-varying path gain G_v observed at 220 (○), 850 (△), and 1900 (●) MHz vs. distance.

the results presented in Sec. IV-A.. Moreover, K falls off with increasing distance, but at a much slower rate than path gain.

The location variability of K is comparable to that of path gain. This can be explained as follows: The location variability of $G = |V|^2 + \sigma^2$ and $K = |V|^2/\sigma^2$ are both dependent on the location variability of $|V|^2$ and σ^2. As we shall show in the next section, the location variability of $|V|^2$ is much greater than σ^2. It thus follows that both G and K have location variabilities that are comparable to that of $|V|^2$ and to each other.

C. Fixed and Time-varying Path Gain vs. Distance

Our second set of reductions involved estimating the fixed path gain G_f (which is proportional to $|V|^2$) and the time-varying path gain G_v (which is proportional to σ^2) which are associated with the time series data collected at each location. These parameters form the numerator and denominator of (4), respectively, so provide insight into the behavior of K. Fixed path gain tends to be dominated by the configuration of obstacles along the direct path between the base and remote terminal while time-varying path gain is largely the result of scattering over a broad range of angles about the remote terminal. Thus, we anticipated that G_f would roll off with distance more quickly and experience greater location variability than G_v. However, few previous studies have either verified or quantified these trends.

We plotted G_f and G_v vs. the distance between the transmitter and receiver at each frequency; the results are presented in Figures 5(a) and (b). Fixed and time-varying path gain both decrease with distance according to a power law relationship. The regression lines for G_f and G_v and the corresponding correlation coefficients and location variabilities in each frequency band are given by

$$\overline{G}_{f,220}(dB) = -33.8\log_{10}d - 90.5;\ \rho = -0.58, \sigma = 7.4, \tag{13}$$

$$\overline{G}_{f,850}(dB) = -37.6\log_{10}d - 110.1;\ \rho = -0.61, \sigma = 7.5, \tag{14}$$

$$\overline{G}_{f,1900}(dB) = -36.9\log_{10}d - 116.9;\ \rho = -0.53, \sigma = 9.1, \tag{15}$$

and

$$\overline{G}_{v,220}(dB) = -25.8\log_{10}d - 116.3;\ \rho = -0.65, \sigma = 4.7, \tag{16}$$

$$\overline{G}_{v,850}(dB) = -32.7\log_{10}d - 122.9;\ \rho = -0.77, \sigma = 4.2, \tag{17}$$

$$\overline{G}_{v,1900}(dB) = -28.4\log_{10}d - 127.4;\ \rho = -0.67, \sigma = 4.9, \tag{18}$$

respectively. Once again, the subscripts indicate the relevant frequency in MHz and all values of σ are given in dB. Also, subscripts have not been added to either ρ or σ; it is understood that the values given with the expression for each regression line apply to that regression line.

Three trends are immediately apparent: (1) At all three frequencies, the fixed path gain falls off with distance a little more quickly than does the time-varying path gain. This, of course, is what causes K-factor to slowly decrease with distance. (2) At all three frequencies, the location variability of time-varying path gain is between 2.5 and 4 dB less than the location variability of the corresponding fixed path gain. This is consistent with our physical understanding of the nature of fixed and time-varying path gains, as summarized earlier in this section. (3) At a given distance, the mean time-varying path gain at each frequency is only a few dB different from those at other frequencies. The differences between the corresponding fixed path gains are far greater.

If one normalizes the path gains by removing the frequency-squared dependence of the free space path loss component, two further trends are apparent: (1) the normalized fixed path gain at lower frequencies is greater than at higher frequencies, likely because diffraction losses are less and (2) the normalized time-varying path gain at lower frequencies is less than at higher frequencies, likely because the obstructions and scatterers in the environment are smaller in terms of wavelength and do not diffract and scatter wireless signals as effectively.

D. Excess Path Gain and Ricean K-factor as a Function of Average Wind Speed

Our third set of data reductions involved determining how path gain and the Ricean K-factor observed at each location are affected by the time-averaged wind speed ν_w in km/h that we observed in the vicinity of the transmitting site. In order to remove the distance dependence from path gain, we calculated the excess path gain ΔG (or the difference in dB) between the path gain G measured at a given location and the mean value $\overline{G}$ observed at that distance. Because Ricean K-factor depends only weakly on distance, and to be consistent with the approach taken by others, we ignored that distance dependence of K and simply compared K to wind speed. The results are presented in Figures 6(a) and (b). The average wind speeds that we observed over all measurements are normally distributed at a significance level of 5%. The mean wind speed was 19 km/h and the standard deviation was 6.7 km/h.

We estimated the regression line that best fits the measured data, the correlation coefficient between each parameter and the average wind speed, and the location variability of the parameter, *i.e.*, the variation of the parameter about the regression line at a given average wind speed. The regression lines for ΔG and K and the corresponding correlation coefficients and location variabilities in each frequency band are given by

$$\Delta\overline{G}_{220}(dB) = -0.037v_W + 0.69;\ \rho = -0.034, \sigma = 7.2, \quad (19)$$

$$\Delta\overline{G}_{850}(dB) = -0.058v_W + 1.11;\ \rho = -0.057, \sigma = 6.9, \quad (20)$$

$$\Delta\overline{G}_{1900}(dB) = 0.001v_W - 0.02;\ \rho = 0.001, \sigma = 7.9, \quad (21)$$

and

$$\overline{K}_{220}(dB) = -0.33v_W + 29.4;\ \rho = -0.26, \sigma = 8.3, \quad (22)$$

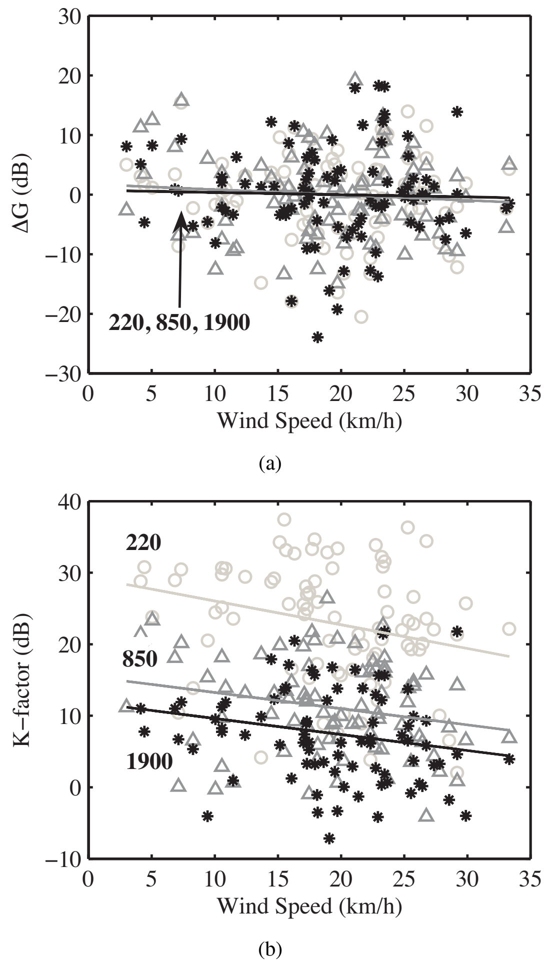

Fig. 6. (a) Excess path gain and (b) Ricean K-factors observed at 220 (○), 850 (△), and 1900 (•) MHz vs. averaged wind speed.

$$\overline{K}_{850}(dB) = -0.23v_W + 15.5;\ \rho = -0.23, \sigma = 6.6, \quad (23)$$

$$\overline{K}_{1900}(dB) = -0.22v_W + 11.9;\ \rho = -0.22, \sigma = 6.8, \quad (24)$$

respectively, where ν_w is expressed in km/h.

As expected, there is no correlation between the excess path gain and the average wind speed. Both the moderate negative correlations between the Ricean K-factor and the average wind speed and the standard deviations at all three frequencies are comparable to each other. The main differences between (22)-(24) are the intercepts of the regression lines with the K axis, which decrease as the carrier frequency increases.

E. Excess Fixed Path Gain and Excess Scatter Path Gain as a Function of Wind Speed

Our fourth set of data reductions involved determining how the fixed and time-varying path gains are affected by the average wind speed. As in the previous section, we eliminated the distance dependence of path gain by taking the excess value of each parameter or the difference (in dB) between the parameter measured at a given location and the mean value observed at that distance. The results are presented in Figures 7(a) and 7(b).

We estimated the regression line that best fits the measured data, the correlation coefficient between each parameter and

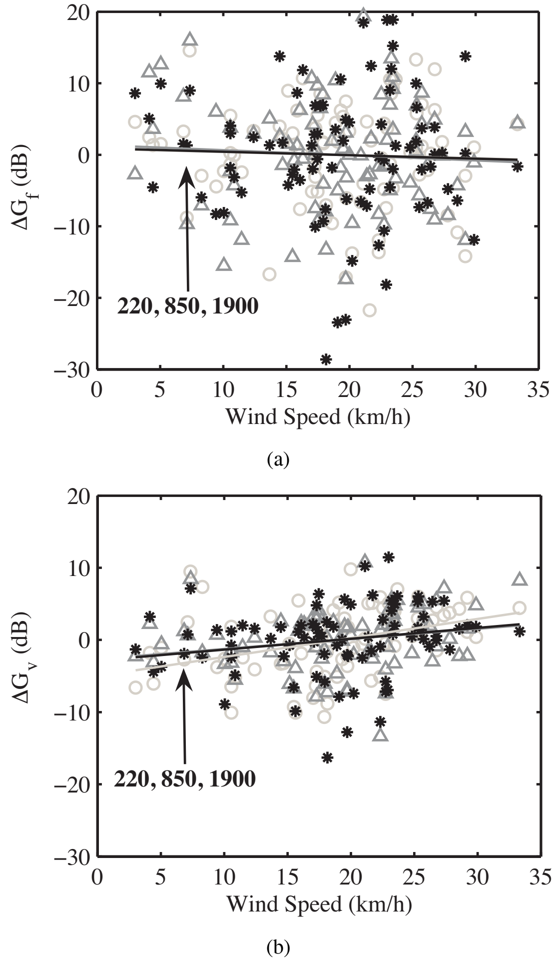

Fig. 7. (a) Excess fixed path gain and (b) excess time-varying path gain observed at 220 (○), 850 (△), and 1900 (●) MHz vs. average wind speed.

the average wind speed, ν_w, and the location variability of the parameter, *i.e.*, the variation of the parameter about the regression line at a given average wind speed. The regression lines for ΔG_f and ΔG_v and the corresponding correlation coefficients and location variabilities in each frequency band are given by

$$\Delta\overline{G}_{f\_220}(dB) = -0.044v_W + 0.84;\ \rho = -0.04, \sigma = 7.4, \tag{25}$$

$$\Delta\overline{G}_{f\_850}(dB) = -0.072v_W + 1.37;\ \rho = -0.064, \sigma = 7.5, \tag{26}$$

$$\Delta\overline{G}_{f\_1900}(dB) = -0.048v_W + 0.9;\ \rho = -0.035, \sigma = 9.1, \tag{27}$$

and

$$\Delta\overline{G}_{v\_220}(dB) = 0.26v_W - 5.0;\ \rho = 0.37, \sigma = 4.7, \tag{28}$$

$$\Delta\overline{G}_{v\_850}(dB) = 0.14v_W - 2.6;\ \rho = 0.22, \sigma = 4.2, \tag{29}$$

$$\Delta\overline{G}_{v\_1900}(dB) = 0.15v_W - 2.9;\ \rho = 0.21, \sigma = 4.9, \tag{30}$$

respectively.

As expected, there is no correlation between the excess fixed path gain and average wind speed. In contrast, there is a clear relationship between time-varying path gain and wind speed. The moderate positive correlations between the excess time-varying path gain and average wind speed at all three frequencies are comparable to each other, as are the standard deviations. The main differences are the intercepts of the regression line with the ΔG_v axis, which generally decreases as the carrier frequency increases.

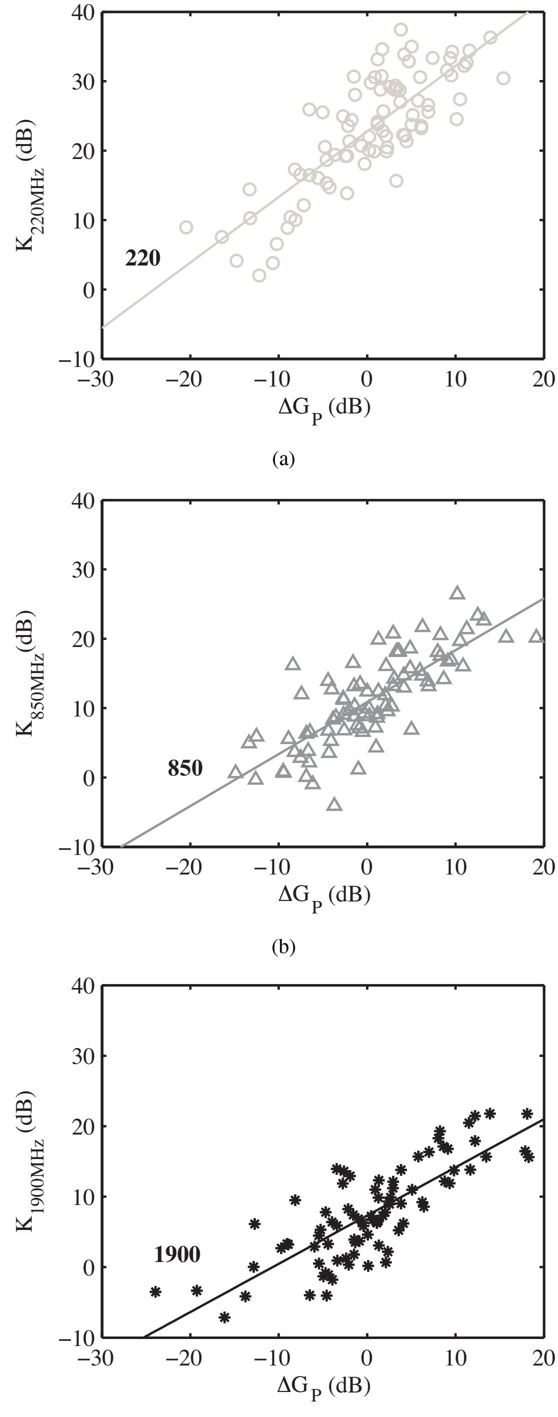

Fig. 8. Scatter plots of Ricean K-factor vs. excess path loss at a given distance at (a) 220 (○), (b) 850 (△), and (c) 1900 (●) MHz.

F. Joint Dependency of the Excess Path Gain and Ricean K-factor

At a given location, we observed a strong correlation between the excess path gain ΔG and the Ricean K-factor. In order to remove distance effects, we replaced K by the excess Rician K-factor ΔK, *i.e.*, the difference in dB between the Rician K-factor observed at a given location and $\overline{K}$ the mean value at that distance which is given by (10)-(12) for the three frequency bands that we considered. The results are presented in Figure 8(a), (b), and (c). The corresponding regression lines are given by

$$\Delta \bar{K}_{220}(dB) = 0.94\Delta G_{220} + 23.1;\ \rho = 0.81, \sigma = 4.9, \quad (31)$$

$$\Delta \bar{K}_{850}(dB) = 0.75\Delta G_{850} + 11.23;\ \rho = 0.78, \sigma = 4.1, \quad (32)$$

$$\Delta \bar{K}_{1900}(dB) = 0.68\Delta G_{1900} + 7.6;\ \rho = 0.80, \sigma = 4.2. \quad (33)$$

Because the dependence of K on distance is so much weaker than its dependence on excess path gain, the correlations given in (31)-(33) are virtually identical to those that we observed between ΔG and K. This correlation between ΔG and ΔK forms the basis for the simulation model that we present in the next section.

V. A Simulation Model

In simulations of fixed wireless systems, it may be necessary to generate values of G and K that a link might experience at a particular frequency and distance. Although we do not have any information concerning the correlation between the values of G and K in either time or space, we can easily generate values that have the same first order statistics as our measured data. In a particular frequency band, we consider G and K as the sum of: (1) the mean value $\overline{G}$ and $\overline{K}$ at a particular distance d and (2) random components ΔG and ΔK which have zero mean. If, as our results suggest, we can assume that ΔG and ΔK are both normally distributed when expressed in dB, their joint distributions are completely described by their mean values, standard deviations and mutual correlation coefficient. Thus, at a given distance and in a specific frequency band, $G(d)$ and $K(d)$ can be generated by

$$\begin{aligned} G\left(d\right) =& \overline{G}\left(d\right) + \Delta G \\ =& \overline{G}\left(d\right) + \sigma_G U_1 \end{aligned} \quad (34)$$

and

$$\begin{aligned} K\left(d\right) &= \overline{K}\left(d\right) + \Delta K \\ &= \overline{K}\left(d\right) + \rho\sigma_K U_1 + \sqrt{1-\rho^2}\sigma_K U_2 \end{aligned} \quad (35)$$

where σ_G is the σ given in (7)-(9), σ_K is the σ given in (10) -(12), ρ is given in (31)-(33), and U_1 and U_2 are uncorrelated Gaussian random variables with zero mean and unit variance.

VI. Conclusions

To the best of our knowledge, this is the first study to compare path gain and signal fading on fixed NLOS links in suburban macrocell environments over the frequency range 220 MHz to 2 GHz. Our most significant finding is that the depth of signal fading drops off rapidly as frequency decreases (or as wavelength increases). A link that experiences severe fading at 1.9 GHz is often relatively unaffected at 220 MHz. An obvious next step for future researchers will be to develop a more sophisticated physical model of such fading that is consistent with the multiband measurement data presented here.

The first-order statistical models that we have presented here capture the essential aspects of the manner in which fixed wireless channels between 200 MHz and 2 GHz fade in a typical suburban macrocell environment. Development of standardized site-general multi-band fading channel models applicable to a broad range of environments would require additional measurement data: (1) from other sites with varying heights and densities of foliage, and with leaves on and off, (2) from transmitters at different heights and (3) at additional frequencies within the range of interest. In combination with existing multi-band path loss models, such multi-band fading channel models will provide a basis for: (1) predicting the coverage and outage probabilities experienced by point-to-multipoint fixed wireless networks deployed in suburban macrocell environments and (2) assessing the suitability of a particular frequency band for use in a given application. The results presented here represent a significant first step toward achieving this goal.

Acknowledgements

We thank BC Hydro Telecom Services for providing us with access to the radio room and rooftop facilities atop Edmonds tower that we used as our transmitting site. We also thank UBC Student Housing and Conferences for providing us with access to the Walter Gage Residence, East Tower during our equipment development and validation runs.

References

[1] W. Webb, “Broadband fixed wireless access as a key component of the future integrated communications environment,” *IEEE Commun. Mag.*, vol. 39, no. 9, pp. 115–121, Sept. 2001.

[2] K. Lu, Y. Qian, and H-H Chen, “Wireless broadband access: WIMAX and beyond,” *IEEE Commun. Mag.,* vol. 45, no. 5, pp. 124–130, May 2007.

[3] S. S. Venkata, A. Pahwa, R. E. Brown, and R. D. Christie, “What future distribution engineers need to learn,” *IIEEE Trans. Power Syst.,* vol. 19, no. 1, pp. 17–23, Feb. 2004.

[4] G. Simard and D. Chartrand, “Hydro-Quebec’s economic and technical approach to justify its distribution automation program,” in *Proc. IEEE PES’07,* pp. 1–5, June 2007.

[5] S. Jim, W. Carr, and S. E. Collier, “Real time distribution analysis for electric utilities,” in *Proc. IEEE REPC’08,* pp. B5–B5-8, Apr. 2008.

[6] D. G. Michelson, V. Erceg, and L. J. Greenstein, “Modeling diversity reception over narrowband fixed wireless channels,” in *Proc. IEEE MTT-TWA’99,* pp. 95–100, Feb. 1999.

[7] L. J. Greenstein, S. S. Ghassemzadeh, V. Erceg, and D. G. Michelson, “Ricean K-factors in narrowband fixed wireless channels: theory, experiments and statistical models,” in*Proc. WPMC’99,* Sept. 1999.

[8] S. Perras and L. Bouchard, “Fading characteristics of RF signals due to foliage in frequency bands from 2 to 60 GHz,” in *Proc. WPMC’02,* pp. 267–271, Oct. 2002.

[9] M. J. Gans, N. Amitay, Y. S. Yeh, T. C. Damen, R. A. Valenzuela, C. Cheon, and J. Lee, “Propagation measurements for fixed wireless loops (FWL) in a suburban region with foliage and terrain blockages,” *IEEE Trans. Wireless Commun,* vol. 1, no. 2, pp. 302–310, Apr. 2002.

[10] E. R. Pelet, J. E. Salt, and G. Wells, “Effect of wind on foliage obstructed line-of-sight channel at 2.5 GHz,” *IEEE Trans. Broadcasting,* vol. 50, no. 3, pp. 224–232, 2004.

[11] D. Crosby, V. S. Abhayawardhana, I. J. Wassell, M. G. Brown, and M. P. Sellars, “Time variability of the foliated fixed wireless access channel at 3.5 GHz,” in *Proc. IEEE VTC 2005 Spring,* pp. 106–110, Sept. 2005.

[12] R. Feick, R. A. Valenzuela, and L. Ahumada, “Experiment results on the level crossing rate and average fade duration for urban fixed wireless channels,” *IEEE Trans. Commun.,* vol. 9, no. 1, pp. 175–179, Jan. 2007.
[13] H. Suzuki, C. D. Wilson, and K. Ziri-Castro, “Time variation characteristics of wireless broadband channel in urban area,” presented at *EuCAP’06,* Nice, France, Nov. 2006.
[14] “Proposals and Changes to the Spectrum in Certain Bands below 1.7 GHz,” Industry Canada Gazette Notice DGTP-004-05, Dec. 2005.
[15] “Policy for the Use of 700 MHz Systems for Public Safety Applications and Other Limited Use of Broadcasting Spectrum,” Industry Canada Radio Systems Policy, RP-006 - Issue 1, June 2006.
[16] M. Hata, “Empirical formula for propagation loss in land mobile radio services,” *IEEE Trans. Veh. Technol.,* vol. 29, no. 3, pp. 317–325, Aug. 1980.
[17] E. Damosso, Ed., “Digital Mobile Radio Toward Future Generation Systems - Final Report,” COST 231 Final Report, 1996.
[18] V. Erceg, L. J. Greenstein, S. Y. Tjandra, S. R. Parkoff, A. Gupta, B. Kulic, A. A. Julius, and R. Bianchi, “An empirically based path loss model for wireless channels in suburban environments,” *IEEE J. Select. Areas Commun.,* vol. 17, no. 7, pp. 1205–1211, July 1999.
[19] Y. H. Lee and Y. S. Meng, “Tropical weather effects on foliage propagation,” in *Proc. EuCAP ’07,* pp. 1–5, Nov. 2007.
[20] L. J. Greenstein, D. G. Michelson, and V. Erceg, “Moment-method estimation of the Ricean K-factor,” *IEEE Commun. Lett.,* vol. 3, no. 6, pp. 175–176, June 1999.
[21] D. S. Baum, D. A. Gore, R. U. Nabar, S. Panchanathan, K. V. S. Hari, V. Erceg, and A. J. Paulraj, “Measurements and characterization of broadband MIMO fixed wireless channels at 2.5 GHz,” in *Proc. IEEE ICPWD’00,* pp. 203–206, Dec. 2000.
[22] S. R. Hanna and J. C. Chang, “Representativeness of wind measurements on a mesoscale grid with station separations of 312 m to 10 km,” *Boundary-Layer Meteorol.,* vol. 60, pp. 309–324, 1992.
[23] D. A. J. Pearce, A. G. Burr, and T. C. Tozer, “Modelling and predicting the fading performance of fixed radio links through vegetation,” in *Proc. IEE NCAP’99,* pp. 263–266, Mar. 1999.
[24] P. Lédl, P. Pechač, and M. Mazánek, “Time-series prediction of attenuation caused by trees for fixed wireless access systems operating in millimeter waveband,” in *Proc. IEE ICAP’03,* pp. 646–649, Mar. 2003.
[25] M. Cheffena and T. Ekman, “Modeling the dynamic effects of vegetation on radiowave propagation,” in *Proc. IEEE ICC’08,* pp. 4466–4471, May 2008.

Anthony Liou received the B.A.Sc. and M.A.Sc. degrees in electrical engineering from the University of British Columbia (UBC), Vancouver, BC, Canada in 2006 and 2009, respectively. His thesis project focused on propagation and channel modeling for fixed wireless communications. He recently joined Universal Scientific Industrial Co., Taiwan where he is working as an engineer-in-training within the RF branch.

Kyle N. Sivertsen received the B.A.Sc. degree in electrical engineering from the University of British Columbia (UBC), Vancouver, BC, Canada in 2007. He is currently a M.A.Sc. candidate with the Department of Electrical and Computer Engineering, UBC. His main research interests include propagation and channel modeling for fixed wireless communications.

Pouyan Arjmandi received the B.A.Sc. degree in electrical engineering from the University of British Columbia (UBC), Vancouver, BC, Canada in 2008. After completing a six-month engineering internship in the Radio Science Lab at UBC in 2008, he joined the business development department at GrowthWorks Capital Ltd, a Canadian venture capital firm that provides funding for technology and life science companies.

Ganapathy Viswanathan received the B.A.Sc. degree in electrical engineering from the University of British Columbia (UBC), Vancouver, BC, Canada in 2008. After completing a six-month engineering internship in the Radio Science Lab at UBC in 2008, he joined Matrikon Inc. where he currently serves as an Industrial Security Consultant to assist the North American Power & Utilities sector to create, implement and manage their Critical Infrastructure Protection (NERC CIP 002-009) program.

Boubacar Diallo received the B.Eng. degree in electrical engineering from the University of Victoria, Victoria, BC, Canada in 2002. Since then, he has been with BC Hydro Telecom Services where he is currently a senior engineer. His main responsibilities include the planning of wireless and fiber optic networks. Mr. Diallo is a registered professional engineer.

Mr. Diallo is currently pursuing a M.A.Sc. degree with the Department of Electrical and Computer Engineering, University of British Columbia, Vancouver, BC Canada on a part-time basis. His main research interests include propagation and channel modeling for smart power grid applications.

Sol Lancashire received the B.A.Sc. degree in electrical engineering from the University of Victoria, Victoria, BC, Canada in 2000. From 2000 until 2008, he was with BC Hydro Telecom Services as a design engineer where he implemented utility telecommunications systems. Since 2008, he has served as BC Hydro’s telecom architect within the Office of the CIO. Mr. Lancashire is a registered professional engineer.

Mr. Lancashire is currently pursuing a M.A.Sc. degree with the Department of Electrical and Computer Engineering, UBC, on a part-time basis. His main research interests include propagation and channel modeling for smart power grid applications.

David G. Michelson (S’80-M’89-SM’99) received the B.A.Sc., M.A.Sc., and Ph.D. degrees in electrical engineering from the University of British Columbia (UBC), Vancouver, BC, Canada.

From 1996 to 2001, he served as a member of a joint team from AT&T Wireless Services, Redmond, WA, and AT&T LabsResearch, Red Bank, NJ, where he was concerned with the development of propagation and channel models for next-generation and fixed wireless systems. The results of this work formed the basis for the propagation and channel models later adopted by the IEEE 802.16 Working Group on Broadband Fixed Wireless Access Standards. From 2001 to 2002, he helped to oversee the deployment of one of the worlds largest campus wireless local area networks at UBC while also serving as an Adjunct Professor with the Department of Electrical and Computer Engineering. Since 2003, he has led the Radio Science Laboratory, Department of Electrical and Computer Engineering, UBC, where his current research interests include propagation and channel modeling for fixed wireless, ultra wideband, and satellite communications.

Prof. Michelson is a registered professional engineer. He serves as the Chair of the IEEE Vehicular Technology Society Technical Committee on Propagation and Channel Modeling and as an Associate Editor for Mobile Channels for IEEE Vehicular Technology Magazine. In 2002, he served as a Guest Editor for a pair of Special Issues of the IEEE JOURNAL ON SELECTED AREAS IN COMMUNICATIONS concerning propagation and channel modeling. From 2001 to 2007, he served as an Associate Editor for the IEEE TRANSACTIONS ON VEHICULAR TECHNOLOGY. From 1999 to 2007, he was the Chair of the IEEE Vancouver Sections Joint Communications Chapter. Under his leadership, the chapter received Outstanding Achievement Awards from the IEEE Communications Society in 2002 and 2005 and the Chapter of the Year Award from IEEE Vehicular Technology Society in 2006. He received the E. F. Glass Award from IEEE Canada in 2009 and currently serves as chair of IEEE Vancouver Section.